Journal of Structural Geology 30 (2008) 1396–1404

Contents lists available at ScienceDirect

Journal of Structural Geology

journal homepage: www.elsevier.com/locate/jsg

Folding kinematics expressed in fracture patterns: An example from the Anti-Atlas fold belt, Morocco

Zeshan Ismat*

Department of Earth and Environment, Franklin and Marshall College, P.O. Box 3003, Lancaster, PA 17604-3003, United States

ARTICLE INFO

Article history:
Received 13 August 2007
Received in revised form 10 July 2008
Accepted 23 July 2008
Available online 12 August 2008

Keywords:
Anti-Atlas
Buckle folds
Dihedral angle
Morocco
Fractures
Valley and Ridge

ABSTRACT

The Anti-Atlas fold belt, Morocco, formed during the same Variscan collisional event that produced the Valley-and-Ridge fold-thrust belt of the Appalachian mountains. Both are external belts of the Appalachian–Ouachita–Mauritanides chain and at the map scale have very similar topographic expressions. The Anti-Atlas, however, consists of map-scale folds that are buckle-related, detachment folds, whereas the Valley-and-Ridge folds developed in response to imbricate thrusting. For this reason, the Anti-Atlas is referred to as a *fold belt* rather than a *fold-thrust belt*.

This paper examines Variscan folding processes in the Anti-Atlas Mountains. Folding in some layers occurred by sliding along a penetrative network of mesoscale fractures, i.e. cataclastic flow, during buckling. Layer-parallel shortening fractures were reactivated in the later stages of folding to accommodate limb rotation. Although 'boutonnieres', i.e. basement uplifts, punctuate the fold belt, the fracture patterns indicate that the uplifts failed to provide any 'bending' component. Folding is also interpreted to occur under low to moderate confining pressures because the fracture network includes conjugate shear fractures with very small (~20°) dihedral angles.

1. Introduction

Under shallow to intermediate crustal conditions, most folds form by buckling, bending (e.g. forced folding), or a combination of both (Cosgrove and Ameen, 2000). Buckling and bending involve tangential longitudinal strain and bed-parallel flexural slip (e.g. Chapple and Spang, 1974; Groshong, 1975; Cooke et al., 2000; Ismat and Mitra, 2005). These two processes can be accommodated by various deformation mechanisms, including fracturing and diffusion (e.g. pressure solution) (Price, 1967; Bayly, 1974; Nickelsen, 1979; Gray and Mitra, 1993; Ismat and Mitra, 2005).

Results from several types of folding models (i.e. theoretical, physical, finite element) have successfully tracked the evolution of natural folds, including the evolution of secondary structures, such as fractures (e.g. Price, 1966; Ramsay, 1967; Bles and Feuga, 1986; Cooke et al., 2000; Ismat and Benford, 2007). The simplest experiments/simulations track folding of *single* competent layers, where complicating factors from the interaction of adjacent competent layers are avoided (e.g. Dieterich, 1970; Friedman et al., 1980; Hunt et al., 1996; Lisle, 2000; Jeng et al., 2002; Johnson and Johnson, 2002; Guiton et al., 2003a,b).

Buckle folds form when the maximum compressive stress is applied approximately parallel to bedding before, and in the early stages of, folding, and perpendicular to the hinge surface as the limbs steepen. Although pure buckle folds are rare in nature, detachment folds are the best (and maybe only) example where folds form by pure buckling. Genuine bend folds, where the local maximum compressive stress is at a high angle or perpendicular to bedding (Ramsay, 1967; Price and Cosgrove, 1990), are similarly rare in nature. Many folds classified as 'bend' folds involve layer-parallel shortening, which suggests some component of buckle folding (Ramsay and Huber, 1987; Cosgrove and Ameen, 2000). Forced, or 'drape', folds are the most commonly described type of bend folds (e.g. Stearns, 1969; Bump, 2004) and form over steep (basement) faults with a minimal component of buckling. Most foreland fold-thrust belts contain fault-bend and fault-propagation folds (Suppe, 1985), both of which involve buckling and bending.

The Anti-Atlas foreland fold belt, Morocco (Fig. 1) is used commonly as a type example for buckle folding (e.g. Guiton et al., 2003a,b; Cartig et al., 2004; Helg et al., 2004; Burkhard et al., 2006). The folds are map-scale detachment folds and so are not cored by duplexes or ramps, which typically contribute a component of bending. Here, the competent units defining the Anti-Atlas fold belt are cored by incompetent shales and are decoupled from adjacent folded competent layers (Cartig et al., 2004; Helg et al., 2004; Burkhard et al., 2006). Unlike other foreland fold belts, the Anti-Atlas contains boutonnieres (i.e. basement inliers) that are similar

* Tel.: +1 717 358 4485; fax: +1 717 291 4186.
E-mail address: zeshan.ismat@fandm.edu

0191-8141/$ – see front matter © 2008 Elsevier Ltd. All rights reserved.
doi:10.1016/j.jsg.2008.07.010

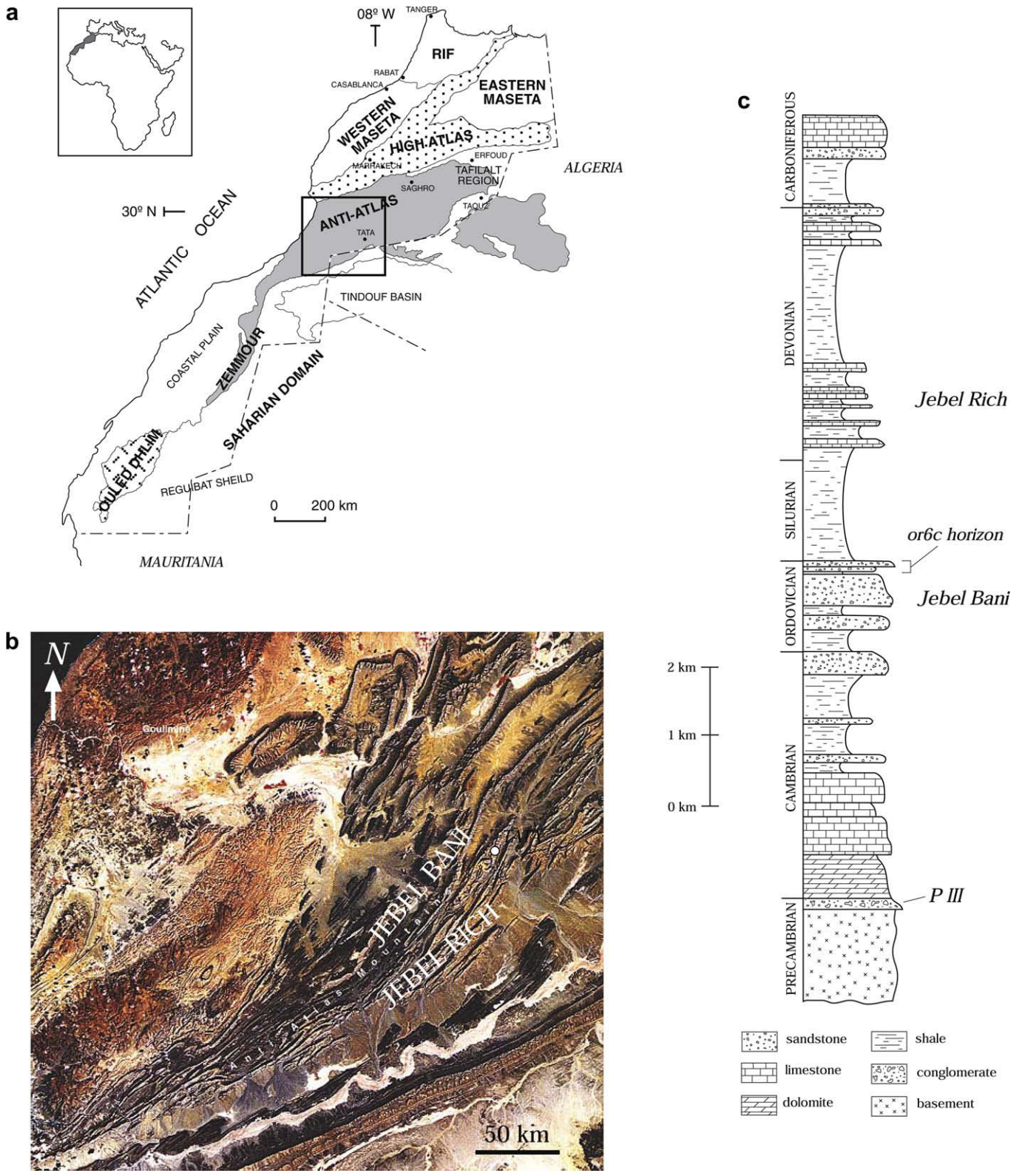

Fig. 1. (a) Map showing location of Anti-Atlas fold belt (shaded gray). (b) Enlarged satellite image from boxed area in part (a) (available at http://zulu.ssc.nasa.gov/mrsid/mrsid.pl). Portion of southwestern Anti-Atlas where fieldwork was conducted. Jebel Bani, Jebel Rich and the city of Tata are labeled. (c) Stratigraphic column from study area.

to the forced, or 'drape', type bend folds of the Wind River-style Laramide basement uplifts, Rocky Mountains, USA (Pique and Michard, 1989; Rodgers, 1995; Cartig et al., 2004; Burkhard et al., 2006). Some models, however, suggest that the boutonnieres are decoupled from the cover folds due to a thick (~1500 m) intervening package of shales, and so do not provide any component of bend folding in the Anti-Atlas fold belt (Helg et al., 2004; Burkhard et al., 2006).

This paper examines the folding processes responsible for the foreland fold belt of the Anti-Atlas Mountains in Morocco. The

fracture patterns preserved in the folded layers are used to determine if the folds are truly pure buckle folds or if there was any bending influence due to the boutonnieres. The Anti-Atlas is used as a case study for several reasons. First, folding occurred at shallow crustal levels (<10 km depth), and was accommodated mainly by fracturing and frictional sliding along a distributed network of fracture sets, i.e. cataclastic flow (Guiton et al., 2003a,b; Cartig et al., 2004; Ismat and Mitra, 2005). Different generations of fractures, and therefore folding stages, can be reconstructed using cross-cutting relationships (e.g. Bott, 1959; Stearns, 1969; Laubscher, 1979; Jamison and Stearns, 1982; Marshak et al., 1982; Hadizadeh and Rutter, 1983; Bles and Feuga, 1986; Laubach, 1988; Ismat and Mitra, 2001, 2005). Second, the Anti-Atlas is comprised of several competent layers that are decoupled from one another by thick sequences of shales/mudstones. Therefore, each layer can be treated as a single-layer fold. Third, the folds span a wide range of interlimb angles. Therefore, the development of fracture patterns can be related to increased fold tightening. The folds are also upright, so complications in strain patterns related to complex fold shapes are avoided. Finally, the outcrops are well exposed and easily accessible.

2. Geology

2.1. Tectonic setting

The Anti-Atlas foreland fold belt is located in southwestern Morocco and is part of the Variscan Appalachian–Ouachita–Mauritanides chain (see Fig. 1a) (Pique and Michard, 1989; Pique et al., 1991; Soulaimani and Pique, 2004). Folding of the Anti-Atlas took place during the middle to late Carboniferous, comparable to the Alleghanian orogeny, which produced the Valley-and-Ridge fold-thrust belt of the Appalachian Mountains (Fig. 2a, b) (Cartig et al., 2004). In general, the Anti-Atlas fold belt trends NE–SW for a length of ~700 km (Fig. 1a). In more detail, the trend of the fold belt changes from NNE–SSW in the southwest to nearly E–W in the northeast, and the number and cylindricity of folds decrease from southwest to northeast (Guiton et al., 2003a,b; Helg et al., 2004; Burkhard et al., 2006). Consequently, the Anti-Atlas fold belt is often subdivided, through the city of Tata (Fig. 1a), into its southwestern and northeastern portions.

Now separated by the Atlantic Ocean, the Anti-Atlas and the Appalachian Valley-and-Ridge often are referred to as a 'paired' belt (Moores and Twiss, 1995) for two reasons. First, both are external belts of the same orogenic belt (Pique et al., 1991; Burkhard et al., 2006). Second, the map-scale fold patterns are strikingly similar, as both form en-echelon and fold v-patterns (Figs. 1b and 2b). However, a major contrast exists in the underlying geometry between the two. The Anti-Atlas is composed of detachment folds whereas the Valley-and-Ridge folds have the classic ramp-flat geometry of foreland fold-thrust belts cored by thrust ramps and duplexes (Nickelsen, 1988; Evans, 1989; Smart and Dunne, 1997; Cartig et al., 2004; Burkhard et al., 2006). Therefore, the Anti-Atlas commonly is referred to as a foreland *fold belt*, rather than a foreland *fold-thrust belt*. Another key difference between the two belts is that, unlike the Valley-and-Ridge, portions of the Anti-Atlas fold belt contain basement inliers, or 'boutonnieres' (Helg et al., 2004).

The differences between the two external belts may be a function of their tectonic and sedimentary setting. The Anti-Atlas is an inverted deep intracratonic basin while the Valley-and-Ridge is a former passive margin of the Paleo-Tethys Ocean (Pique and Michard, 1989; Burkhard et al., 2006). The Anti-Atlas folds are composed of a vast package of marine sediments with thick layers of shale (Fig. 1c). As a result, thin competent layers of sandstone and limestone are mechanically decoupled from other competent layers via thick shale units, and so the competent layers defining the Anti-Atlas fold trains behave essentially as 'single-layer' folds.

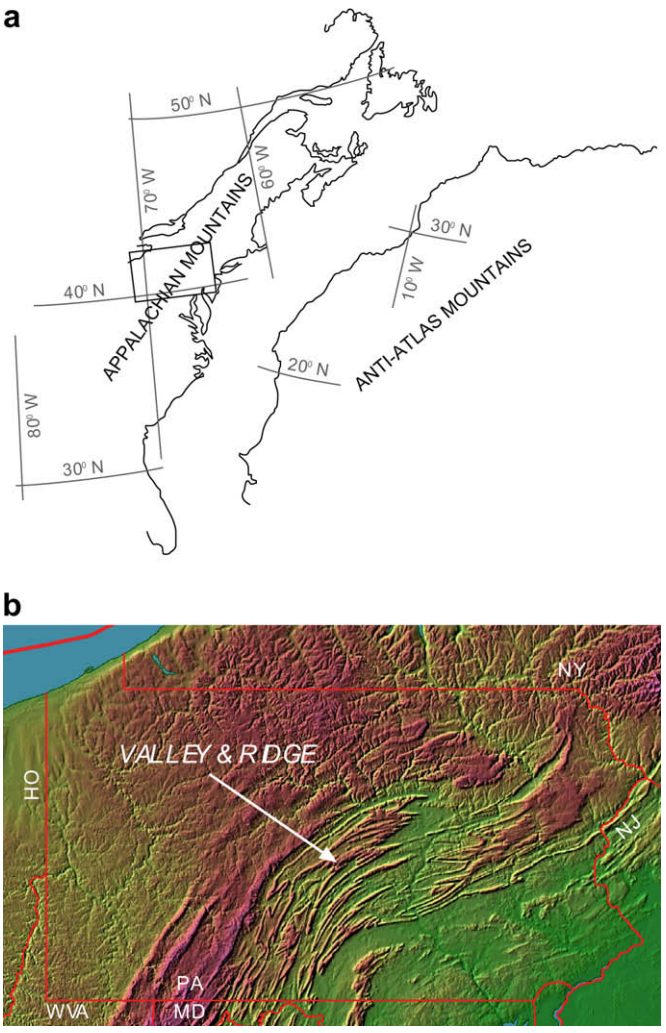

Fig. 2. Map showing relative positions of North America and Africa during the Variscan collisional event that produced the Anti-Atlas and Valley-and-Ridge, Appalachia. Modern latitude and longitudinal lines shown (after LePichon et al., 1977). (b) Enlarged satellite map from boxed area in (a) (available at http://www.virginiaplaces.org/boundaries/graphics/pa.gif). Note fold v-patterns in the Valley-and-Ridge province.

The folded sedimentary cover sequence of the Anti-Atlas overlies Precambrian basement rocks (Fig. 3). During the Variscan orogeny, buckle folding of the sedimentary cover was likely concurrent with uplift of the underlying basement blocks, forming the present day boutonnieres (Helg et al., 2004; Burkhard et al., 2006). These basement blocks were uplifted along reactivated extension faults that originally formed during opening of the Iapetus Ocean (precursor to the Atlantic Ocean).

2.2. Folded units

The stratigraphic package of interest in the Anti-Atlas fold belt ranges from the lower Cambrian to the middle Carboniferous. The units consist of competent sandstones and limestones with thick intervening layers of incompetent shales (Fig. 1c). The sedimentary cover is ~10–12 km in thickness in the southwestern Anti-Atlas but ~6–8 km in the northeastern portion of the fold belt (Destombes et al., 1985; Villeneuve and Cornee, 1994; Pique, 2001; Helg et al., 2004). The folded competent layers form thin, continuous marker beds that outline the fold geometry (Fig. 1).

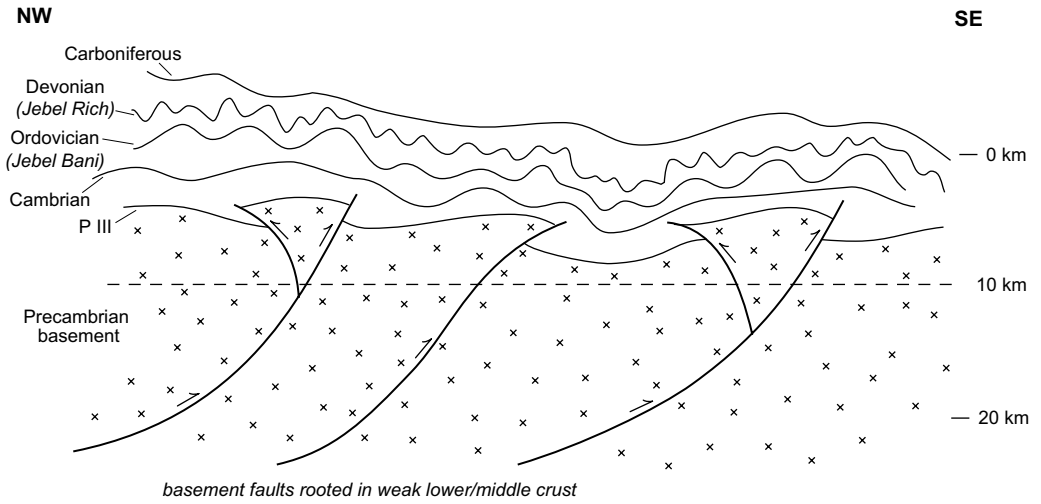

Fig. 3. Schematic cross-section through the Anti-Atlas Mountains. Adapted from Cartig et al. (2004).

Two main fold trains that define the Anti-Atlas, the Jebel Bani and the Jebel Rich, are composed of Ordovician sandstones and Devonian limestones, respectively (Figs. 1b, c and 3). These fold trains are decoupled from each other, due to thick intervening Silurian shales (Fig. 1c). Although the two fold trains have the same fold style, their wavelengths vary, most likely due to the varying thicknesses of the sandstone and limestone layers, and so form polyharmonic folds (Fig. 3) (Burkhard et al., 2006). The Jebel Bani is comprised of a series of sandstone layers with a total thickness of up to ~500 m and the wavelength of the Bani folds range from 3 to 5 km. The limestones comprising the Jebel Rich have an average thickness of ~100–200 m and the fold wavelengths are ~1 km (Helg et al., 2004). In addition, fold amplitudes in the Jebel Bani are much larger than in the Jebel Rich (Burkhard et al., 2006).

This paper focuses on the southwestern portion of the Anti-Atlas where the folds are better exposed and preserve a wider range of fold geometry than in the northeast (Fig. 1b). Here, the Jebel Bani and the Jebel Rich trend ~030° ± 10° and are comprised of upright folds with very low plunges (<30°). The fold limbs in individual folds dip uniformly, ranging from ~10° to ~80° for both sets of fold trains. More specifically, this paper concentrates on the Jebel Bani. Because the Jebel Bani is composed primarily of sandstones, deformation generally is accommodated by fracturing and not diffusional mass transfer, as seen commonly in the limestones of the Jebel Rich.

The sandstone layers of the Jebel Bani vary slightly in grain size and amount and type of impurities. Recent work has shown that slight lithological variations cause significant differences in fracture geometry (Ismat and Mitra, 2005), so the data presented here are only from the uppermost sandstone layer, the or6c horizon (or 2nd Bani) (Fig. 1c) (Helg et al., 2004). This choice permits lithologically independent comparisons of fracture patterns between various field sites. The or6c horizon is a microconglomeratic sandstone with a thickness ranging from only 50 to 90 m, forms prominent dip slopes, and is easily accessible throughout the field area (Fig. 4).

3. Fracture patterns

Restored balanced cross-sections reveal that folding of the Anti-Atlas occurred at a depth of ≤10 km, within the elastico-frictional regime (Sibson, 1977; Burkhard et al., 2006). During fold tightening within the elastico-frictional regime, fracture patterns can evolve and this evolution is most clearly documented by cross-cutting relationships between fracture sets (Ismat and Mitra, 2005). The simple fold geometry within the Anti-Atlas offers an ideal place to track changes in fracture development and reactivation. The microconglomeratic sandstone that is the focus of this study contains abundant fractures with cross-cutting relationships (Fig. 4), and these structures are the primary outcrop-scale features that developed during fold evolution.

3.1. Data collection

Fracture sets were measured from ~55 sites across the limbs and hinges of folds whose limb dips range from ~10° to ~75°. Within any single fold, fractures were measured on at least three sites in the limbs and a minimum of two sites in the hinge region. The sites described in this paper are representative sites for a range of limb dips in the folds.

At each site, ~50 fractures were measured within two mutually perpendicular ~2 m^2 area grids; the fracture sets are abundant and statistically homogeneous at this scale (Fig. 4). Two mutually perpendicular area grids were used to characterize the fracture patterns in three-dimensions. All fractures were measured within each 2 m^2 area to capture the complex and bulk characteristics of the fractured rocks (Price, 1967). Cross-cutting relationships were used to identify the youngest, or *active*, fractures. Morphological descriptions were recorded for both active and older fractures. Fractures were weighted in terms of abundance, trace-length, and fault zone thickness. The weighted active fractures from all of the

Fig. 4. Outcrop fracture patterns, from the Jebel Bani, looking NW.

sites were normalized so that direct comparisons could be made between sites. The example in Fig. 5 is used to illustrate each step of this weighting process.

For abundance, each fracture occurrence is a weighting of one as a function of orientation. These counts accumulate to identify the most abundant fracture orientations. The poles to the fractures are illustrated as a scatter plot (Fig. 5a) and a contoured equal-area plot (Fig. 5b). At all of the sites, all of the fracture trace-lengths were divided by the shortest trace-length to create a normalized size distribution. The smallest value in the normalized range is one, which was given a weighting factor of 1. Larger normalized values were weighted by the multiple of how much longer that fracture was relative to the smallest active fracture. In addition, at all sites, the widths of fault zones were divided by the smallest width to create normalized size ranges. The smallest value in each normalized range is one, which was given a weighting factor of 1. Larger normalized values were weighted by the multiple of how much thicker that fault zone was relative to the thinnest active fault zone.

The three weighting factors were added at each site for each fracture set to identify the fracture sets that had the largest combination of abundance, fracture lengths and fault zone widths. The weighted poles to the fracture sets were then contoured on equal-area nets (Fig. 5c). The most common fracture sets were determined from the pole concentrations and plotted as great circles (Fig. 5d) (Ismat and Mitra, 2001).

3.2. Results

Fracture sets are subdivided into three groups: A, B and C (Figs. 6 and 7). Set A is most prominent. These are mode I fractures, or joints, that range in length from 1 to 2 m, are steeply dipping to vertical with a strike sub-perpendicular to the overall NE–SW trend of the folds, and commonly have plumose patterns and/or twist hackles on the fracture surface (Fig. 8). Set B forms single and double conjugate sets of steeply dipping faults, or shear fractures that are generally less than 1 m in length. The acute bisector of Set B faults is parallel to Set A joints. Set C is the least abundant and is commonly found in the outer-arc region of the folds. These form single faults and joints or conjugate sets of faults that are moderate to steeply dipping, strike at a high angle to fracture Set A, i.e. strike approximately parallel to the fold hinge, and are approximately 1 m in length. Slickenlines, often multiple sets, are commonly found along Sets B and C. The slickenlines along fault Sets B are generally close to being parallel to the fracture–bedding intersection, whereas the slickenlines on Sets C are commonly sub-parallel to the fracture's dip direction. Earlier work on fracture sets within the Jebel Rich near this field area reveal similar sets of slickenline patterns on conjugate fractures (Guiton et al., 2003a,b). Here, I have observed both single and double sets of conjugate fractures.

4. Data interpretation

4.1. Fracture patterns

In the early stages of folding, Set A joints formed parallel to the maximum compressive stress whereas Set B faults accommodated shortening parallel to bedding, typically with single conjugate sets. Set C fractures accommodated outer-arc extension and postdate both Sets A and B. These fracture geometries occur in both hinges and limbs of the host folds. They are consistent with patterns that were previously identified for single-layer buckle folds (Hancock, 1985; Nickelsen, 1988; Price and Cosgrove, 1990; Macktelow and Abassi, 1992; Cortes, 2000). They are not consistent with patterns for bending folds because they are not concentrated in hinge zones (Ameen, 1990, 1992). Also, if bending dominated, perhaps due to emplacement of the basement boutonnieres, the common fracture patterns should also consist of joints parallel to the fold hinge and reveal a change in fracture patterns around the fold with different fold geometries (Ameen, 1990, 1992; Richard, 1991; Wicks et al., 2000). None of these patterns are observed in the Bani folds. The proposed buckle folding with concurrent fracturing might have been simultaneous with basement inversion, but the thick package of shale between the basement and cover rocks is inferred to have decoupled the fold belt from the boutonnieres so that buckling rather than bending conditions dominated in the folded or6c horizon (Figs. 1c and 3) (Burkhard, 2006).

4.2. Shortening directions

The shortening directions, determined from the acute bisector of the conjugate faults, or the intersection of the acute bisectors of conjugate–conjugate faults (Angelier, 1979; Reches, 1978, 1983; Reches and Dieterich, 1983), are also consistent with buckle folding models. Set B faults are used to establish the shortening directions in fold limbs during folding. Set C faults are not used because they are in the outer arcs of the folds, have low abundance and hence, they do not provide information on the overall kinematic history of the folds.

During the early stages of folding ($\lesssim 30^\circ$ limb dips), the shortening direction is sub-horizontal, as would be expected from buckle folds. Beyond $\sim 30^\circ$, an additional conjugate set of Set B faults (Set B_2, Fig. 7) formed whose acute bisector trends at a high angle to the acute bisector of the earlier formed Set B faults (Set B_1, Fig. 7). This new conjugate set formed under the same stress field that formed Set A joints and the initial Set B_1 faults, i.e. with the

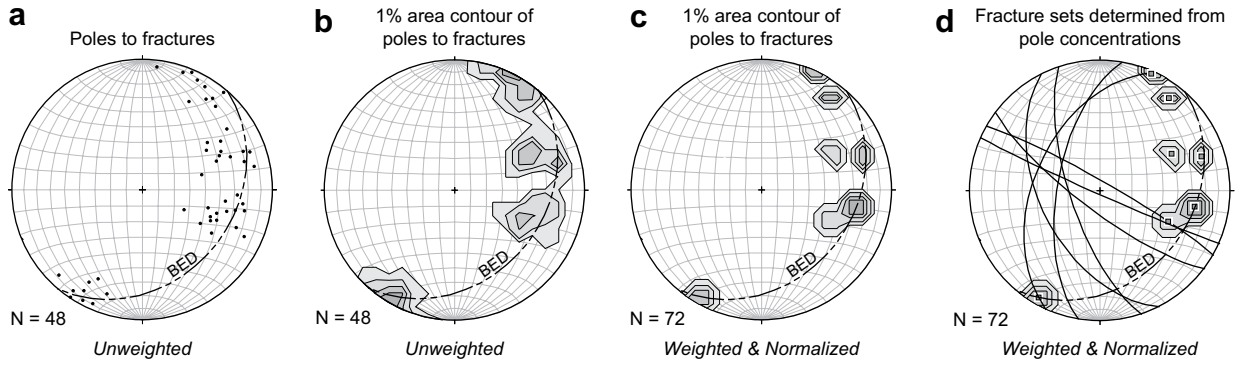

Fig. 5. Example (from the east limb) illustrating how fracture sets were weighted. (a) Scatter plot and (b) 1% area contour of poles to fractures showing fracture abundance. (c) 1% area contour of poles to weighted fractures. (d) Fracture sets (great circles) chosen from the weighted pole concentrations.

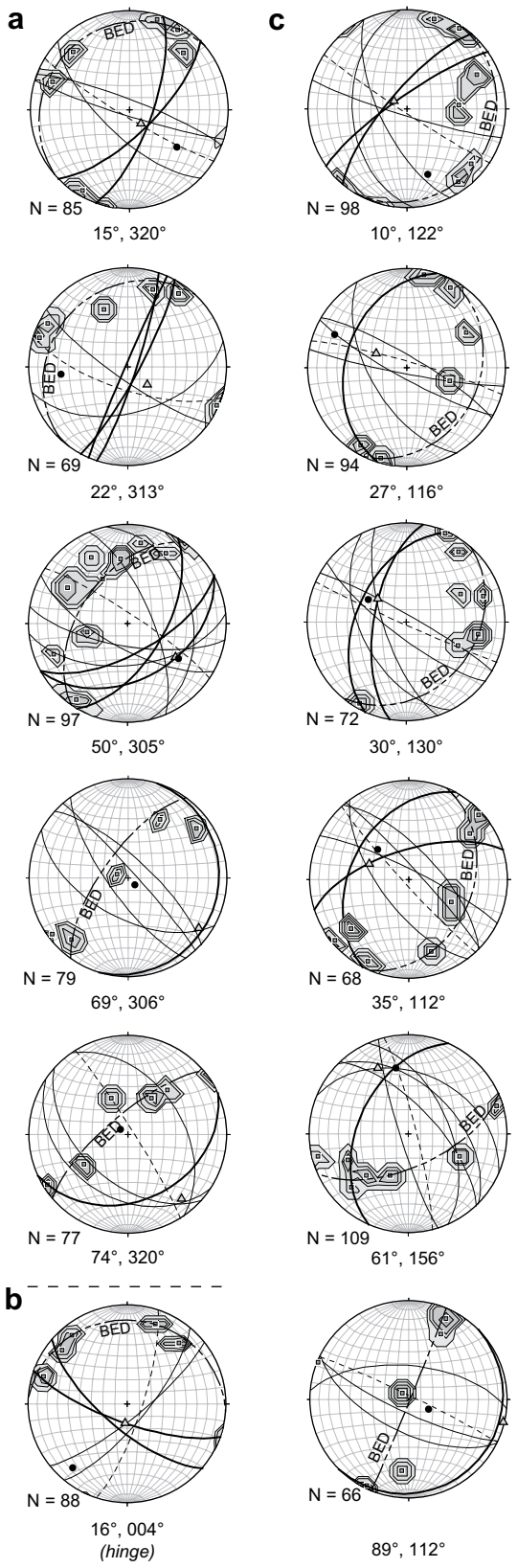

Fig. 6. (a–c) Representative fracture patterns from the (a) west limb (b) hinge region and (c) east limb of the Jebel Bani folds represented on equal-area nets. Bedding orientation is given as dip, dip direction and is represented as a semi-dashed great circle with label 'BED'. Poles to fractures are contoured at 1% intervals. Black circle shows maximum shortening direction, determined from Set B faults, and gray triangle is the pole to bedding. Great circles are subdivided into three groups, representing three different fracture sets. The dashed great circle represents fracture Set A, the solid thin great circle represents Set B and the thick black great circle represents Set C. The same patterns are used in Fig. 7.

maximum compressive stress oriented sub-perpendicular to the hinge surface. All of the Set B faults are mutually cross-cutting, which suggests that the earlier formed set, B_1, was reactivated with renewed slip. The shortening direction determined from the combined Set B faults for limb dips between ~30° and ~60° is at a high angle to bedding, which is expected as the limbs steepen and rotate during folding. Once the limbs steepen to dips $\gtrsim$60°, the acute bisector becomes parallel to bedding, i.e. sub-vertical. The orientation of the slickenlines on the Set B fracture surfaces suggest that the mesoscale fracture-bound blocks slid past each other parallel to the dip direction of the beds, i.e. sub-vertically. This suggests that the earlier formed fractures are now reactivated to accommodate limb rotation and extension (Nickelsen, 1979; Bles and Feuga, 1986; Ismat and Benford, 2007). Therefore, the acute bisector during the late stages of folding represents the maximum *extension* direction.

Although Set B_1 conjugate faults and Set B_2 conjugate faults were both active during the later stages of folding, they did not form at the same time. Therefore, these two conjugate sets of faults are not referred to here as 'conjugate–conjugate' sets (Reches, 1978). Instead, Sets B_1 and B_2 faults are called a 'double set of conjugate faults', which does not presume any timing information on the formation of the fault sets.

4.3. Bed-parallel slip

Evidence for bed-parallel slip, via slickenlines, may be preserved in both buckle and bend folds. These slickenlines, however, are best developed (i.e. more abundant and continuous) in different locations for each case (Dubey and Cobbold, 1977; Ameen, 1988; Cooke et al., 2000). Although bedding plane slickenlines are observed throughout the limbs of the Jebel Bani folds, they are best developed in limbs that dip between 35° and 45°. A similar bed-parallel slip pattern is preserved in the Canyon Range syncline, part of the Sevier foreland fold-thrust belt, USA (Ismat and Mitra, 2005). According to Byerlee (1978), pre-existing surfaces (e.g. bedding) oriented ~41° to the maximum compressive stress (or shortening) direction will be reactivated under confining pressures typically produced within the upper crust (Ismat and Mitra, 2005). So, with a sub-horizontal maximum compressive stress, as would be required to form buckle folds, surfaces oriented at ~41° are expected to slide most easily. In forced-type bend folds, however, slickenlines are expected to be best developed in the hinge region and gradually decrease away from the hinge region (Ameen, 1988; Cosgrove and Ameen, 2000), which is not observed in the Bani folds. Therefore, the location of the best developed slickenlines within the Jebel Bani supports the hypothesis that they are buckle folds.

5. Conjugate–conjugate fracture patterns: small dihedral angle

Using confining pressure as a proxy for depth, joints, such as Set A, are expected to form under shallower crustal levels than conjugate faults (Paterson, 1978; Ramsey and Chester, 2004). The dihedral angle for both of the conjugate fault Sets B and C averages only ~20° (Fig. 9), which differs from the dihedral angle for typical conjugate sets of faults of ~50° to ~60° (Handin, 1969; Paterson, 1978; Reches, 1983; Hancock, 1985; Mandl, 2000). Recent experimental work has shown that the angle between conjugate sets decreases with a decrease in confining pressure (Ramsey and Chester, 2004). So, these small acute angles are interpreted to imply

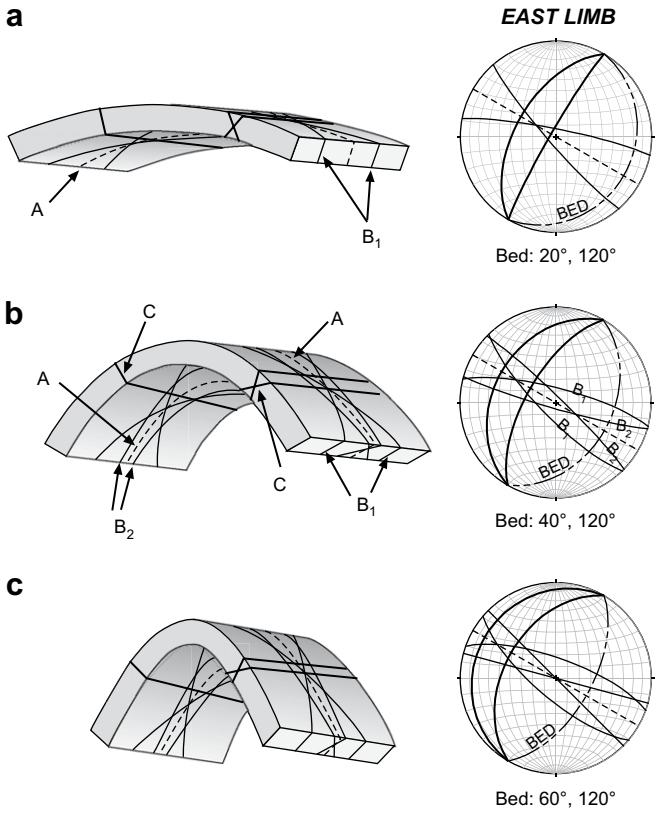

Fig. 7. Three-dimensional fold models showing orientations of average fracture sets preserved in the Jebel Bani. Folds are trending 030°/210°. Fracture sets are represented as great circle patterns on equal-area nets for (a) 20° (b) 40° (c) and 60° bedding dips for the east limb. The same line patterns are used in the fold models and in the equal-area nets.

Fig. 8. Twist hackle from a Set A fracture.

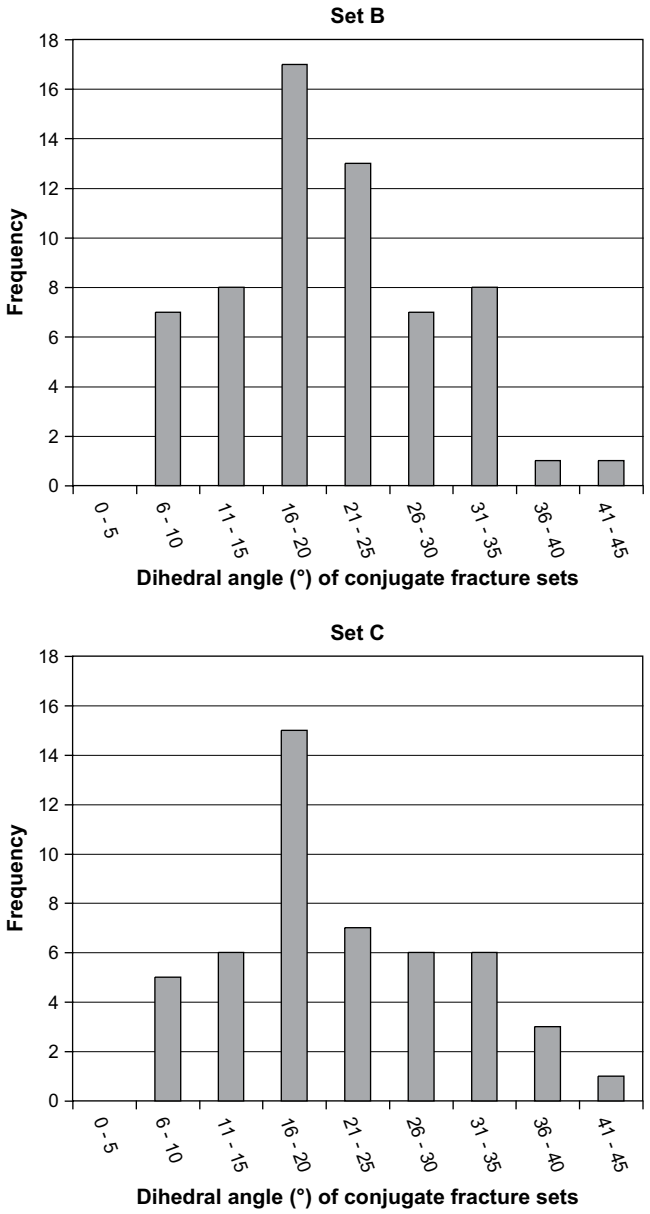

Fig. 9. Frequency histograms for the dihedral angles of conjugate fractures from (a) Set B and (b) Set C.

that the confining pressure during fault formation is consistent with relatively shallow crustal conditions.

Restored cross-sections from the southwestern Anti-Atlas reveal that the or6c horizon was at a maximum depth of only ~6 km during folding (Fig. 1c) (Burkhard, 2006). This depth equates to a confining pressure of only 150 MPa (based on a vertical stress gradient of ~25 MPa/km) (Means, 1976), which is low for conjugate fault formation and high for joint formation (Paterson, 1978; Middleton and Wilcock, 1994; Ramsey and Chester, 2004).

Set A joints and the initial Set B_1 faults formed during the early stages of folding. Their orientations suggest that they formed with a maximum compressive stress applied approximately parallel to bedding and so indicate that the folds formed by buckling. If the Set A joints and the Set B_1 (conjugate) faults did form during the same stage of folding, the Anti-Atlas may in fact preserve a unique range of confining pressure that spans the upper limit of extensional fracture formation and the lower limit of shear fracture formation. This range is likely very small and therefore rarely preserved. Additionally, it may be difficult to recognize the timing of fracture formation in some cases because as folding continues, different combinations of fracture sets may be reactivated to continue fold tightening by cataclastic flow.

6. Conclusion

1. Fracturing and frictional sliding along a distributed network of fractures, in other words, cataclastic flow, accommodated folding of the Anti-Atlas fold belt.

2. The shortening direction progressively changes from approximately parallel to bedding for gentle limb dips (<30°) to a high angle to bedding for limb dips between ~30° and ~60°. This pattern is expected for folds that form by buckling. Beyond limb dips of ~60°, the fracture sets are reactivated to accommodate limb rotation and extension.
3. Although portions of the fold belt are punctuated by 'boutonnieres' (i.e. basement uplifts), the fracture patterns show no influence that they formed as a consequence of bend folding. The folded cover sequence was likely decoupled from the underlying basement by a thick package of incompetent shales.
4. Set A joints and Set B_1 (conjugate) faults formed during the initial stage of folding. If both sets did form near simultaneously, the Anti-Atlas may preserve a unique range of confining pressures that spans the upper limit of extensional fracture formation and the lower limit of shear fracture formation.

Acknowledgements

I thank the reviewers, Michele Cooke and Gary Lash, for their helpful and thoughtful comments. I also thank the editor, William Dunne, for his patience and detailed comments. This manuscript benefited from discussions with Gautum Mitra. Finally, I am indebted to Martin Burkhard and his two former graduate students, Severine Cartig and Charles Robert-Charrue, for their help and wonderful discussions in the field. Support was provided by NSF-SGER grant EAR-0318906 and a Woodrow Wilson Career Enhancement fellowship.

References

Ameen, M.S., 1988. Folding of Layered Cover Due to Dip-slip Basement Faulting. PhD thesis, University of London.
Ameen, M.S., 1990. Macrofaulting in the Purbeck-Isle of Wight monocline. Proceedings of the Geologists Association 101, 31–46.
Ameen, M.S., 1992. Strain pattern in the Purbeck-Isle of Wight monocline, a case study of folding due to dlip-slip in the basement. In: Bartholomew, M.J., Hyndman, D.W., Mogk, D.W., Mason, R. (Eds.), Characterization and Comparison of Ancient (Precambrian–Mesozoic) Continental Margins. Proceedings of the 8th International Conference on Basement Tectonics at Butte, MT, USA. Kluwer, Dordrecht, pp. 559–578.
Angelier, J., 1979. Determination of the mean principal stress from a given fault population. Tectonophysics 56, T17–T26.
Bayly, M.B., 1974. An energy calculation regarding the roundness of folds. Tectonophysics 24, 291–316.
Bles, J.L., Feuga, B., 1986. The Fracture of Rocks. Elsevier, Amsterdam.
Bott, M.H.P., 1959. The mechanics of oblique slip faulting. Geological Magazine 96, 109–116.
Bump, A.P., 2004. Three-dimensional Laramide deformation of the Colorado Plateau; competeing stresses from the Sevier thrust belt and the flat Farallon slab. Tectonics 23.
Burkhard, M., Cartig, S., Helg, U., Robert-Charrue, C., Soulaimani, A., 2006. Tectonics of the Anti-Atlas of Morocco. Comptes Rendus Geosciences 338, 11–24.
Byerlee, J., 1978. Friction of rocks. Pure and Applied Geophysics 116, 615–626.
Cartig, S., Burkhard, M., Docummum, R., Helg, U., Kopp, L., Sue, C., 2004. Fold interference patterns in the Late Paleozoic Anti-Atlas belt of Morocco. Terra Nova 16, 27–37.
Chapple, W.M., Spang, J.H., 1974. Significance of layer-parallel slip during folding of layered sedimentary rocks. Geological Society of America Bulletin 85, 1523–1534.
Cooke, M.L., Mollema, P.N., Pollard, D.D., Aydin, A., 2000. Interlayer slip and joint localization in the East Kaibab Monocline, Utah: field evidence and results from numerical modeling. In: Cosgrove, J.W., Ameen, M.S. (Eds.), Forced Folds and Fractures. Geological Society, London, Special Paper, vol. 169, pp. 23–49.
Cortes, P., 2000. Mecanismes et caracterisation de la fracturation de mode 1 dans les roches stratifies: terraines et experimentation. Doctoral thesis, University of Montpellier II, France.
Cosgrove, J.W., Ameen, M.S., 2000. A comparison of the geometry, spatial organization and fracture patterns associated with forced folds and buckle folds. In: Cosgrove, J.W., Ameen, M.S. (Eds.), Forced Folds and Fractures. Geological Society, London, Special Paper, vol. 169, pp. 7–21.
Destombes, J., Hollard, H., Willefret, S., 1985. Lower Paleozoic rocks of Morocco. In: Holland, C.H. (Ed.), Lower Paleozoic of North-Western and West-Central Africa. Trinity College, Department of Geology, Dublin, Ireland, pp. 91–336.
Dieterich, J.H., 1970. Computer experiments on mechanics of finite amplitude folds. Canadian Journal of Earth Sciences 7, 467–476.
Dubey, A.K., Cobbold, P.R., 1977. Noncylindrical flexural slip folds in nature and experiment. Tectonophysics 38, 223–239.
Evans, M.A., 1989. The structural geometry and evolution of foreland thrust systems, northern Virginia. Geological Society of America Bulletin 101, 339–354.
Friedman, M., Hugman, R.H.H., Handin, J., 1980. Experimental folding of rocks under confining pressure, part VIII: forced folding of unconsolidated sand and of lubricated layers of limestone and sandstone. Geological Society of America Bulletin 91, 307–312.
Gray, M.B., Mitra, G., 1993. Migration of deformation fronts during progressive deformation: evidence from detailed structural studies in the Pennsylvania Anthracite region, USA. Journal of Structural Geology 15, 435–449.
Groshong, R.H., 1975. Strain, fractures and pressure solution in natural single-layer folds. Geological Society of America Bulletin 86, 1363–1376.
Guiton, M.L.E., Leroy, Y.M., Sassi, W., 2003a. Activation of diffuse discontinuities and folding of sedimentary layers. Journal of Geophysical Research 108 (B4) ETG 3-1–ETG 3-20.
Guiton, M.L.E., Sassi, W., Leroy, Y.M., Gauthier, B.D.M., 2003b. Mechanical constraints on the chronology of fracture activation in folded Devonian sandstone of the western Moroccan Anti-Atlas. Journal of Structural Geology 25, 1317–1330.
Hadizadeh, J., Rutter, E.H., 1983. The low temperature brittle–ductile transition in a quartzite and the occurrence of cataclastic flow in nature. Geologische Rundschau 72, 493–509.
Hancock, P.L., 1985. Brittle microtectonics: principles and practice. Journal of Structural Geology 7, 437–457.
Helg, U., Burkhard, M., Cartig, S., Robert-Charrue, C., 2004. Folding and inversion tectonics in the Anti-Atlas of Morocco. Tectonics 23 (TC4006), 1–17.
Handin, J., 1969. On the Coulomb-Mohr failure criterion. Journal of Geophysical Research 74, 5343–5348.
Hunt, G., Muhlhaus, H., Hobbs, B., Ord, A., 1996. Localized folding of visco-elastic layers. Geologische Rundschau 85, 58–64.
Ismat, Z., Mitra, G., 2001. Folding by cataclastic flow at shallow crustal levels in the Canyon Range, Sevier orogenic belt, west-central Utah. Journal of Structural Geology 23, 355–378.
Ismat, Z., Mitra, G., 2005. Folding by cataclastic flow: evolution of controlling factors during deformation. Journal of Structural Geology 27, 2181–2203.
Ismat, Z., Benford, B., 2007. Deformation in the core of a fold: unraveling the kinematic evolution of tight, multilayer folds developed in the upper crust. Journal of Structural Geology 29, 497–514.
Jamison, W.R., Stearns, D.W., 1982. Tectonic deformation of the Windgate Sandstone, Colorado National Monument. American Association of Petroleum Geologists 66, 2584–2608.
Jeng, F.S., Lin, M.L., Lai, Y.C., Teng, M.H., 2002. Influence of strain rate on buckle folding of an elasto-viscous single layer. Journal of Structural Geology 24, 501–516.
Johnson, K.M., Johnson, A.M., 2002. Mechanical analysis of the geometry of forced folds. Journal of Structural Geology 24, 401–410.
Laubach, S.E., 1988. Fractures generated during folding of the Palmerton Sandstone, eastern Pennsylvania. Journal of Geology 96, 495–503.
Laubscher, H.P., 1979. Elements of Jura kinematics and dynamics. Eclogae Geologicae Helvetiae 72, 467–483.
LePichon, X., Sibuet, J.C., Francheteau, J., 1977. The fit of the continents around the North Atlantic Ocean. Tectonophysics 38, 169–209.
Lisle, R.J., 2000. Predicting patterns of strain from three-dimensional fold geometries: neutral surface folds and forced folds. In: Cosgrove, J.W., Ameen, M.S. (Eds.), Forced Folds and Fractures. Geological Society, London, Special Paper, vol. 169, pp. 213–221.
Macktelow, N.S., Abbassi, M.R., 1992. Single layer buckle folding in non-linear materials. II. Comparison between theory and experiment. Journal of Structural Geology 14, 105–120.
Mandl, G., 2000. Faulting in Brittle Rocks: an Introduction to the Mechanics of Tectonic Faults. Springer.
Marshak, S., Geiser, P.A., Alvarez, W., Engelder, T., 1982. Mesoscopic fault array in the northern Umbrian Apennine fold belt, Italy: geometry of conjugate shear by pressure solution. Geological Society of America Bulletin 93, 1013–1022.
Means, W.D., 1976. Stress and Strain: Basic Concepts of Contiuum Mechanics for Geologists. Springer-Verlag, New York.
Middleton, G.V., Wilcock, P.R., 1994. Mechanics of the Earth and Environmental Sciences. Cambridge University Press.
Moores, E.M., Twiss, R.J., 1995. Tectonics. W.H. Freeman and Company, New York.
Nickelsen, R.P., 1979. Sequence of structural stages of the Allegheny orogeny, at the Bear Valley strip mine, Shamokin, Pennsylvania. American Journal of Science 279, 255–271.
Nickelsen, R.P., 1988. Structural evolution of folded thrust and duplexes on a first-order anticlinorium in the Valley and Ridge Province of Pennsylvania. In: Mitra, G., Wojtal, S. (Eds.), Geometries and Mechanics of Thrusting. Geological Society of America, Special Paper, vol. 222, pp. 89–106.
Paterson, M.S., 1978. Experimental Rock Deformation – the Brittle Field. Springer, Berlin.
Pique, A., 2001. Geology of Northwest Africa. Gebruder Borntrager, Stuttgart, Germany.
Pique, A., Michard, A., 1989. Moroccan hercynides: a synopsis: the Paleozoic sedimentary and tectonic evolution at the northern margin of West Africa. American Journal of Science 289, 286–330.
Pique, A., Cornee, J.J., Muller, J., Roussel, J., 1991. The Moroccan hercynides. In: Dallmeyer, R.D., Lecorche, J.P. (Eds.), The West African Orogens and Circum Atlantic Correlatives. Springer-Verlag, New York, pp. 229–263.

Price, N.J., 1966. Fault and Joint Development in Brittle and Semi-Brittle Rock. Pergamon Press, London.
Price, R.A., 1967. The tectonic significance of mesoscopic subfabrics in the southern Rocky Mountains of Alberta and British Columbia. Canadian Journal of Earth Sciences 4, 39–70.
Price, N.J., Cosgrove, J.W., 1990. Analysis of Geological Structures. Cambridge University Press.
Ramsay, J.G., 1967. Folding and Fracturing of Rocks. McGraw Hill.
Ramsay, J.G., Huber, M.I., 1987. The Techniques of Modern Structural Geology, Volume 2: Folds and Fractures. Academic Press, New York.
Ramsey, J.M., Chester, F.M., 2004. Hybrid fracture and the transition from extension fracture to shear fracture. Nature 428, 63–66.
Reches, Z., 1978. Analysis of faulting in three-dimensional strain field. Tectonophysics 47, 109–129.
Reches, Z., 1983. Faulting of rocks in three-dimensional strain fields: II. Theoretical analysis. Tectonophysics 95, 133–156.
Reches, Z., Dieterich, J.H., 1983. Faulting of rocks in three dimensional strain fields: 1. Failure of rocks in polyaxial, servo-control experiments. Tectonophysics 95, 111–132.
Richard, P., 1991. Experiments on faulting in a two layer cover sequence overlying a reactive basement fault with oblique slip. Journal of Structural Geology 13, 459–470.
Rodgers, J., 1995. Lines of basement uplifts within the external parts of orogenic belts. American Journal of Science 295, 455–487.
Sibson, R.H., 1977. Fault rocks and fault mechanics. Journal of the Geological Society of London 133, 191–213.
Smart, K.J., Dunne, W.M., 1997. Roof sequence response to emplacement of the Wills Mountain duplex: the roles of forethrusting and scales of deformation. Journal of Structural Geology 19, 1443–1459.
Soulaimani, A., Pique, A., 2004. The Tasrirt structure: a Late Pan-African transtensive dome. Journal of African Earth Science 39, 247–255.
Stearns, D.W., 1969. Fracture as a mechanism of flow in naturally deformed layered rocks. In: Proceedings, Conference on Research in Tectonics, Geological Survey of Canada Paper 68-52, pp.79–96.
Suppe, J., 1985. Principle of Structural Geology. Prentice Hall, New Jersey.
Villeneuve, M., Cornee, J.J., 1994. Structure, evolution and paleogeography of the West African Craton and bordering belts during the Neoproterozoic. Precambrian Research 69, 307–326.
Wicks, J.L., Dean, S.L., Kulander, B.R., 2000. Regional tectonics and fracture patterns in the Fall River Formation (Lower Cretaceous) around the Black Hills foreland uplift, western South Dakota and northeastern Wyoming. In: Cosgrove, J.W., Ameen, M.S. (Eds.), Forced Folds and Fractures. Geological Society, London, Special Paper, vol. 169, pp. 145–165.